**Solid Freeform Fabrication 2024: Proceedings of the 35th Annual International Solid Freeform Fabrication Symposium – An Additive Manufacturing Conference**
**Reviewed Paper**

# Predicting the fatigue life of multi-jet fusion fabricated polyamide 11 ankle-foot orthosis: Durability insights from S-N curve analysis

Ryan Blakis* and Mladenko Kajtaz*

*School of Engineering, RMIT University, PO Box 71, Bundoora, Victoria 3083, Australia.

Email: ryan.blakis@student.rmit.edu.au

## Abstract

In this study, we assessed the fatigue performance of HP Multi-Jet Fusion (MJF) polyamide 11 (PA11), specifically targeting its application in 3D-printed ankle-foot orthoses (AFO). We produced an S-N curve to characterize the material's endurance under cyclic flexural stress by performing fully reversed flexural fatigue tests according to ASTM D7774. To test the accuracy of the S-N curve in predicting the fatigue life of the AFOs, we subjected a 3D-printed AFO to fatigue testing that replicated real-world stresses. Our results demonstrated a correlation between the S-N curve predictions and the actual performance of the 3D-printed AFO, providing crucial insights into the life of HP MJF fabricated orthoses subject to fatigue. This study offers a foundation for further research and development in 3D-printed AFOs, highlighting the importance of fatigue characterization in ensuring patient safety and device durability.

## Introduction

An ankle-foot orthosis (AFO) is a passive external device prescribed to children and adults to support the ankle-foot complex and improve gait patterns affected by neuromuscular disorders [1–3]. Traditional custom AFOs are manually designed and fabricated using a vacuum thermoforming method, shaping heated thermoplastic over a plaster mold derived from a patient cast [4]. Rigid AFOs are a design variant that aim to block all motion of the ankle during gait. The AFO is considered rigid enough if dorsiflexion movement is limited to less than $3^\circ$ during the second rocker of gait [5].

Ankle rigidity, commonly referred to as ankle stiffness, is defined by the AFO angle-moment relationship measured in Newton-meters per degree of ankle rotation ($\mathrm{N\,m}/^\circ$) [6]. Ankle stiffness is predicted prior to manufacture with computational techniques like finite element analysis (FEA), or evaluated post manufacture via bench-testing with custom fixtures or functional analysis [7, 8]. Achieving sufficient rigidity with traditional manufacturing methods requires using thick materials and conservative trim lines around the ankle, resulting in heavy devices with extensive low-stress areas. These low-stress areas are not easily optimized when conventional manufacturing methods are employed. In contrast, 3D printing enables design optimization by producing innovative designs that are not restricted by traditional manufacturing limitations. This allows for improved aesthetics, comfort, and significant weight reduction, while still achieving the desired mechanical performance [9, 10]. Additionally, manufacturing lead times can be shortened from weeks to days [11]. Despite these benefits, a drawback of the layer-by-layer build method is an increased susceptibility to mechanical fatigue failure [12]. This is particularly problematic in applications like AFOs, which are subjected to cyclic loading.

Fatigue is a type of damage that occurs due to cyclic loading, leading to progressive structural degradation even when the applied loads are much lower than the material's yield strength [12–14]. In polymers, fatigue failure can occur through two mechanisms: thermal fatigue and mechanical fatigue [15, 16]. A key difference between dynamic fatigue in metals and

polymers is the role of cyclic frequency. Due to their viscoelasticity, high damping, and low thermal conductivity, polymers experience temperature increases influenced by both loading frequency and stress levels, making them prone to softening from hysteretic heating [17,18]. Additionally, parts produced through additive manufacturing are more susceptible to mechanical fatigue due to weaker interlayer bonds, surface roughness, and internal defects such as porosity and voids, which act as stress concentrators and crack initiation sites. However, some additive manufacturing methods can reduce these vulnerabilities more effectively than others.

Multi Jet Fusion (MJF), a powder bed fusion technique developed by HP, produces components with good mechanical properties, low anisotropy, and minimal porosity [19–22]. These qualities are likely to reduce the risk of failure under repeated loading. While extensive research has examined the mechanical properties of MJF polyamide-11 (PA11) under quasi-static loading, there is a lack of investigation into its behavior under dynamic loading and the interlayer failures commonly seen in other additive methods. This gap also applies to the context of cyclic loading in AFO geometries.

This study addresses the need to understand the mechanical properties of MJF PA11 under dynamic loading, with a special focus on cyclic loading for AFO geometry. Using the S-N curve, we aim to predict the durability of an MJF fabricated AFO, offering valuable insights into the material's performance under such conditions.

## Materials and methods

The method proposed in this research was developed on the key idea that the S-N curve can be used to predict the durability of an MJF fabricated AFO. To evaluate this, the method includes three distinct steps: (i) development of a high cycle fatigue S-N curve for MJF PA11 under flexural loading conditions, (ii) prediction of stress distribution and peak magnitudes in an AFO by employing computational prediction models, and (iii) conducting fatigue testing on an MJF fabricated AFO.

### Materials

PA11 powder (commercial name: HP 3D High Reusability PA11) was used, with the following properties: particle size of $54\,\mu m$, melting point of $202\,^{\circ}C$ and print density of $1.05\,g/cm^3$.

### Test specimen preparation

Test specimens and the AFO were fabricated in separate batches using an HP MJF 3D 4200 printer. The printer's build volume was $380\,mm \times 284\,mm \times 380\,mm$. The "balanced" print mode was employed to optimize a compromise between appearance, dimensional accuracy, and mechanical properties. All parts were centered in the build volume, with $10\,mm$ to $20\,mm$ spacing between each part to ensure complete thermal flow. Parts were printed using PA11 powder with proprietary fusing and detailing agents provided by HP. The PA11 powder had a $70\,\%$ new to $30\,\%$ old refresh ratio, as recommended by HP. Parts were oriented with their length aligned with the sweep direction of the IR source. After printing, the parts were allowed to cool in the powder bed for $16\,h$ before being unpacked. Loose powder was recycled, and the printed specimens were cleaned using bead blasting and air blasting.

## AFO design

Ankle-foot orthosis geometry was generated using Rhino 7 and Grasshopper [23]. The method employed was inspired by Dal Maso & Cosmi (2019) [2], and consisted of generating a surface model from a reference 3D scan by lofting cross-sections, then trimming the scan with additional surfaces to leave only the AFO geometry. The origin of the model was defined as the midpoint of the line between the apices of the medial and lateral malleoli using the Talus Coordinate System [24]. Trimming surfaces were constructed by extruding curves from the mid-plane. For this study, the medial and lateral trimming surfaces were made identical to reduce complexity in the design. The final trimmed surface was thickened to the common thickness of 4 mm [25], and exported as an STL file for 3D printing. The surface geometry of the AFO was exported as a STEP file for the FEA study. The artificial limb was constructed using the same method but with a different trimming surface.

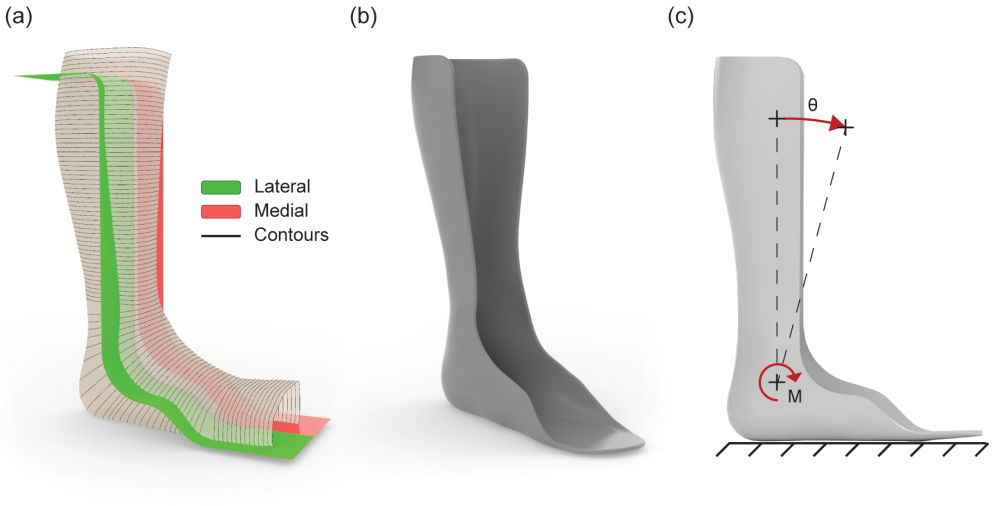


Figure 1: (a) AFO geometry generation workflow highlighting section contours and trimming surfaces (b) Render of thickened AFO (c) Key boundary conditions for second ankle rocker of gait loading in FEA study

## AFO test rig

To experimentally characterize the ankle stiffness and conduct fatigue testing, a specialized test rig was developed as shown in Figure 2. The test rig was designed to be configured to interface with an Instron universal test system, or, be a standalone system. To achieve this, a crank slider mechanism was used to convert linear translational motion into rotational motion. The linear motion actuation was connected to a load cell in both configurations. The moment applied around the ankle joint in the sagittal plane is calculated based on mechanism geometry and measured reaction force.

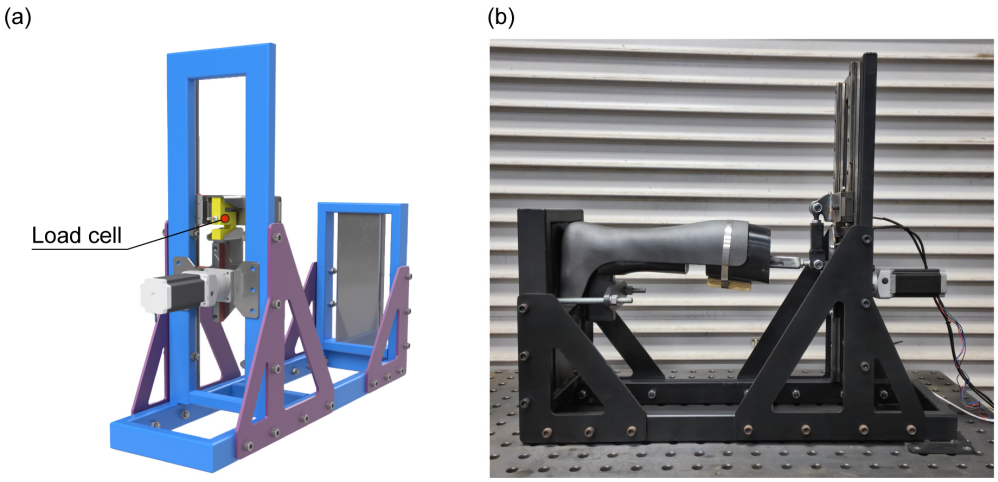


Figure 2: (a) Test rig standalone configuration highlighting load cell position (b) Test rig with 3D printed AFO fitted for testing

**Experimental characterization techniques**

Mechanical property testing for quasi-static three-point bending flexure was conducted with an Instron universal test instrument, Model 5900R with $5\,\text{kN}$ load cell. Dynamic fully reversed three-point bending was performed with an Instron universal test instrument, Model E3000 with $3\,\text{kN}$ load cell.

Flexural testing was performed with a three-point bending test fixture using specimens with rectangular cross-section of $12.7\,\text{mm}\times3.2\,\text{mm}$ in accordance with ASTM D790-17 [26]. Specimens were $100\,\text{mm}$ in length to provide sufficient overhang for the support distance of $51.2\,\text{mm}$. Testing was conducted in accordance with procedure A and B, with crosshead speeds of $1.365\,\text{mm/min}$ and $13.65\,\text{mm/min}$ for a strain rates of $0.01\,\text{mm/mm/min}$ and $0.1\,\text{mm/mm/min}$ respectively. Tests were conducted at ambient temperature.

Dynamic flexural testing was performed using specimens of rectangular cross-section of $12.7\,\text{mm}\times3.2\,\text{mm}$ in accordance with ASTM D7774-17 [27]. The load controlled fully reversed bending ($R = -1$) was performed for several load amplitudes, derived from the stress-strain response observed during quasi-static flexural testing. The test-end was defined as $10^6$ cycles, with early test termination occurring due to rupture or yielding. Yielding was defined as 10% or more increase in deflection to achieve the target stress amplitude as outlined in ASTM D7774-17. Testing was conducted at $5\,\text{Hz}$ at ambient temperature.

Fatigue testing of the AFO consisted of cyclic loading reflective of the second ankle rocker of gait for $10^6$ cycles, reflective of approximately $12$ months use. The load cycle consisted of rotating the AFO from the neutral position to a rotation that induced a target peak stress about the ankle axis. Testing was conducted at a frequency of $3\,\text{Hz}$. Due to hardware limitations, continuous load cell measurements could not be taken at the cyclic loading rate. Consequently, the test program was designed to slow down every one thousand cycles to perform quasi-static characterization, conducted at the rotational load rate of $16.2\,^\circ/\text{min}$.

### Finite element analysis

Finite element analysis was used to identify the rotation at which the target peak stress magnitude occurred in the AFO. This was achieved using a load case reflective of the second rocker of gait as depicted in Figure 1(c) [8, 10, 28]. The static analysis was conducted using the commercial FEA software ABAQUS CAE from Dassault Systèmes [29]. MJF PA11 was modeled using the native ABAQUS elastic-plastic combined hardening material model [30].

The AFO and partial artificial limb geometry were modeled as surfaces and discretized in ABAQUS employing the free meshing technique. Shell elements S4R and S3 were assigned to the AFO, while the artificial limb was defined as a 3D discrete rigid shell. The additional geometry representing the partial limb was included to mitigate excessive unrealistic buckling of the AFO above the ankle at the trim line. The artificial limb geometry was connected to the calf reference point using a rigid body constraint. This reference point was then linked to the ankle reference point with a wire, upon which a revolute connector constraint was applied. The calf reference point was linked to a partitioned section of the internal surface of the AFO that represented the calf cuff through a kinematic coupling. The contact between the AFO and the limb was defined as frictionless.

A static general load step was created, with nonlinear geometry (nlgeom) enabled. The load case, as illustrated in Figure 1(c), fixed the underside of the foot plate in all six degrees of freedom (DOF) with an appropriate boundary condition. Rotation about the virtual ankle joint was generated by applying a moment, iteratively sized to induce the target peak stress. A mesh sensitivity study was conducted until the peak stress converged within $2\,\%$, resulting in an element seed size of $2\,\mathrm{mm}$.

## Results & discussion

The results and discussion section presents the data collected during our study, accompanied by detailed analysis highlighting key findings and their implications. This section is divided into the three sections outlined in the methodology.

### S-N curve

The mechanical properties of MJF PA11 were experimentally characterized by conducting quasi-static and dynamic flexure tests. Quasi-static flexure tests were conducted at two speeds as outlined in ASTM D790-17, with stress-strain relationships presented in Figure 3(a). Enhanced mechanical performance consistent with typical polymer behavior was observed at the higher strain rate [31]. Although the stress-strain response was initially linear, considerable nonlinearity was exhibited, with a transition occurring approximately between $3\,\%$ and $4\,\%$ flexural strain. No specimens ruptured before reaching the $5\,\%$ flexural strain test limit.

The quasi-static test results were used to define the initial stress amplitude of $36\,\mathrm{MPa}$ for the fully reversed flexural fatigue testing. This stress amplitude was selected as the starting stress amplitude as it was positioned in the early onset of the observed nonlinear stress-strain response. Among the three specimens tested at this stress amplitude, the lowest performing specimen failed at $2.27 \times 10^5$ cycles, which was within the high cycle fatigue range. It should be noted that the test end condition for all failed specimens was triggered due to a $10\,\%$ increase in displacement to achieve the target stress amplitude, and not due to rupture. On inspection, these specimens showed no visible signs of damage, suggesting the possibility of degradation in

stiffness due to thermal causes. Subsequently, a stress amplitude of 31 MPa, marking the end of the linear stress-strain response, was tested. All three specimens withstood the designated test limit of $10^6$ cycles. Testing at 33 MPa resulted in two of the three specimens enduring until the test conclusion. These results suggest that the stress amplitude at which the desired stress-life of $10^6$ cycles lies between 31 MPa and 33 MPa. The obtained results were used to produce the S-N curve presented in Figure 3(b), with individual results presented in Table 1. Due to equipment availability, testing was limited to three stress amplitudes rather than the four recommended by ASTM D7774-17.

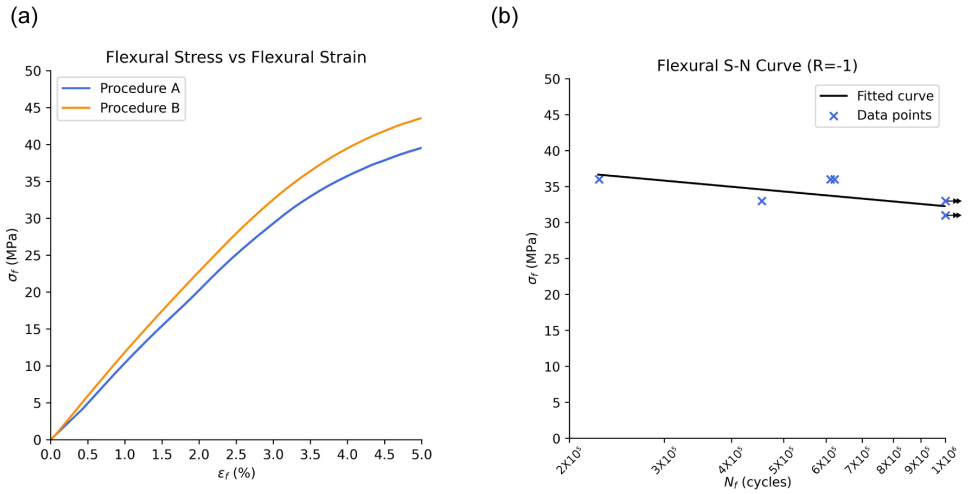


Figure 3: (a) Flexural stress-strain curve for MJF PA11 (b) S-N curve for flexural fatigue for MJF PA11

Table 1: Flexural fatigue results (ASTM D7774)

| **Stress amplitude (MPa)** | **#1** | **#2** | **#3** |
|---|---|---|---|
| 31 | $1 \times 10^6$ | $1 \times 10^6$ | $1 \times 10^6$ |
| 33 | $4.55 \times 10^5$ | $1 \times 10^6$ | $1 \times 10^6$ |
| 36 | $2.27 \times 10^5$ | $6.11 \times 10^5$ | $6.22 \times 10^5$ |

**Stress prediction**

Finite element analysis was employed to determine the rotation angle at which the target peak stress of 32 MPa occurred in the AFO. The analysis revealed that the AFO experienced a peak stress of 31.84 MPa at 2.6° of rotation. Figure 4(a) illustrates the stress distribution, highlighting a pronounced stress concentration along the trim line surrounding the malleolus region, observed on both the medial and lateral sides of the AFO. This concentration is attributed to "frog mouthing", a phenomenon whereby the AFO opens outwards during ankle dorsiflexion. Frog mouthing was observed to become more considerable after approximately 1.5° of dorsiflexion rotation, with the extent of this local deformation at 2.6° highlighted by the deformation plot in Figure 4(b). Significantly, the plot also demonstrates how the AFO closes inwards above the malleolus, confirming the need to include limb geometry in AFO simulations.

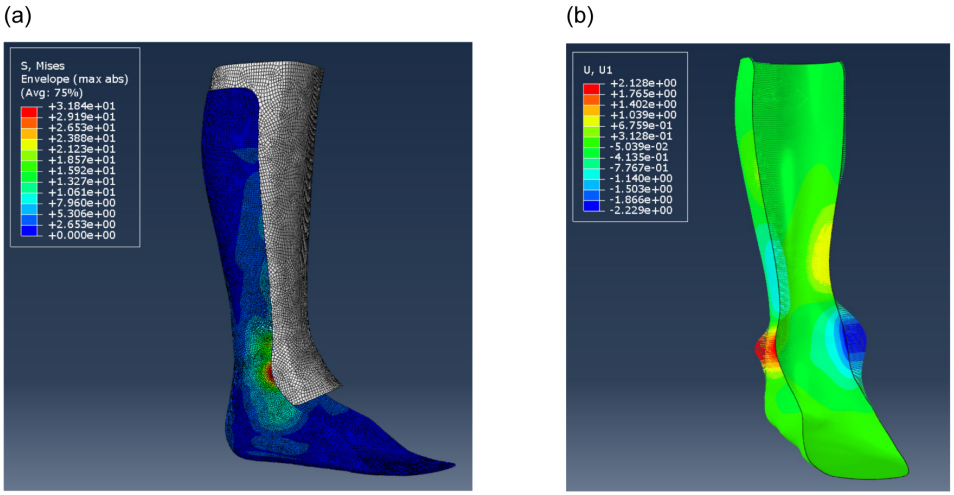


Figure 4: (a) Stress distribution in the AFO at $2.6°$ of rotation (b) Local deformation in the AFO trim line around the malleolus

## Fatigue

The AFO underwent one million load cycles, with an enforced rotation of $2.6°$ as determined by the FEA study. The AFO did not rupture during testing; however, as shown in Figure 5(a), the ankle stiffness decreased by a total of $23\,\%$. A significant portion of this stiffness degradation occurred within the first two hundred thousand load cycles, after which the stiffness appeared to stabilize, with only minor additional degradation over the remaining cycles. To explore this behavior further, loading and unloading profiles from the first and last cycles were compared (Figure 5(b)). A stable response was initially exhibited in the load profiles, characterized by consistent reaction moment magnitudes within the $0°$ to $0.75°$ range. The divergence observed outside this region was likely due to localized changes from accumulated damage, leading to increased hysteresis and stiffness degradation. This theory is supported by the FEA study, which identified significant stress concentrations at the trim line around the malleolus, a region demonstrated to significantly contribute to rotational stiffness [32]. The hypothesis of localized damage suggests a potential underprediction of peak stresses by the FEA model and/or application-specific behavior not captured by the S-N curve. Future investigations should focus on more comprehensively characterizing dynamic material behavior and conducting additional fatigue testing on diverse AFO geometries at varied stress amplitudes. Enhancing predictive accuracy through these means is essential for a thorough assessment of performance under cyclic loading conditions.

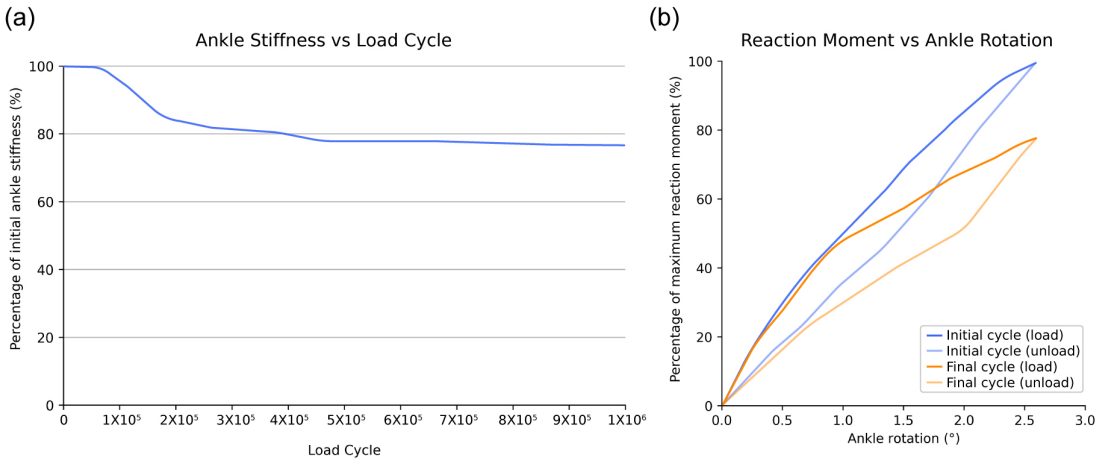


Figure 5: (a) Ankle stiffness vs load cycle number (b) Load profile of first and last load cycles

## Conclusion

This study generated an S-N curve for MJF PA11 and used it to design a MJF-fabricated AFO intended to last one million load cycles. The S-N curve, developed according to ASTM D7774-17, identified an endurance limit between 31 MPa and 33 MPa. Finite element analysis was then used to predict the rotation angle at which the target peak stress of 32 MPa would occur in the simulated AFO. The fabricated AFO underwent experimental testing under cyclic loading conditions simulating the second ankle rocker phase of gait, reaching the predicted rotation over one million load cycles. The tested AFO did not fail by rupture, however, a reduction in ankle stiffness of approximately 23 % was observed. Additionally, differences in the loading-unloading reaction moment profile were noted between the first and last load cycles after $0.75^\circ$ of rotation, possibly due to localized damage in high-stress regions near the malleolus trim line. This suggests that the FEA model may be underestimating peak stresses, or that the S-N curve might not fully capture certain application-specific behaviors. These preliminary findings, particularly the absence of rupture, indicate that MJF-fabricated AFOs are durable under cyclic in-service loading. Incorporating this method into the design workflow for 3D-printed AFOs, regardless of the printing method, could enhance long-term performance and reliability, as demonstrated by this study.

## Acknowledgements

The authors would like to thank *The Footwork Podiatric Laboratory*, Melbourne, Australia for providing the test specimens and sharing their facilities with us.

## References

[1] Sarah F. Tyson and Ruth M. Kent. Effects of an Ankle-Foot Orthosis on Balance and Walking After Stroke: A Systematic Review and Pooled Meta-Analysis. Archives of Physical Medicine and Rehabilitation, 94(7):1377–1385, 7 2013.

[2] Alberto Dal Maso and Francesca Cosmi. 3D-printed ankle-foot orthosis: a design method. Materials Today: Proceedings, 12:252–261, 1 2019.

[3] Elizabeth Wojciechowski, Angela Y. Chang, Daniel Balassone, Jacqueline Ford, Tegan L. Cheng, David Little, Manoj P. Menezes, Sean Hogan, and Joshua Burns. Feasibility of designing, manufacturing and delivering 3D printed ankle-foot orthoses: a systematic review. Journal of Foot and Ankle Research, 12(1):11, 12 2019.

[4] Dequan Zou, Tao He, Michael Dailey, Kirk E. Smith, Matthew J. Silva, David R. Sinacore, Michael J. Mueller, and Mary K. Hastings. Experimental and computational analysis of composite ankle-foot orthosis. Journal of Rehabilitation Research and Development, 51(10):1525–1536, 2014.

[5] Stefania Fatone, Elaine Owen, Fan Gao, Garth Shippen, Michael S. Orendurff, and Kristie Bjornson. Comparison of Sagittal Plane Stiffness of Nonarticulated Pediatric Ankle-Foot Orthoses Designed to be Rigid. JPO Journal of Prosthetics and Orthotics, 34(1):e44–e49, 1 2022.

[6] D.J.J. Bregman, A. Rozumalski, D. Koops, V. de Groot, M. Schwartz, and J. Harlaar. A new method for evaluating ankle foot orthosis characteristics: BRUCE. Gait & Posture, 30(2):144–149, 8 2009.

[7] Toshiki Kobayashi, Aaron K. L. Leung, and Stephen W. Hutchins. Techniques to measure rigidity of ankle-foot orthosis: A review. The Journal of Rehabilitation Research and Development, 48(5):565, 2011.

[8] Alessio Ielapi, Malcolm Forward, and Matthieu De Beule. Computational and experimental evaluation of the mechanical properties of ankle foot orthoses. Prosthetics & Orthotics International, 43(3):339–348, 6 2019.

[9] Anton du Plessis, Chris Broeckhoven, Ina Yadroitsava, Igor Yadroitsev, Clive H. Hands, Ravi Kunju, and Dhruv Bhate. Beautiful and Functional: A Review of Biomimetic Design in Additive Manufacturing, 5 2019.

[10] Ryan Blakis, Peter Dabnichki, and Mladenko Kajtaz. A novel generatively designed and additively fabricated ankle-foot orthosis. In Y.M Xie, J Burry, T.U Lee, and J Ma, editors, Proceedings of the IASS Annual Symposium 2023 Integration of Design and Fabrication, pages 1411–1421, Melbourne, 2023.

[11] Roland K. Chen, Yu-an Jin, Jeffrey Wensman, and Albert Shih. Additive manufacturing of custom orthoses and prostheses—A review. Additive Manufacturing, 12:77–89, 10 2016.

[12] Hamed Bakhtiari, Muhammad Aamir, and Majid Tolouei-Rad. Effect of 3D Printing Parameters on the Fatigue Properties of Parts Manufactured by Fused Filament Fabrication: A Review. Applied Sciences, 13(2):904, 1 2023.

[13] Wolfgang Grellmann and Sabine Seidler. Mechanical Properties of Polymers. In Wolfgang Grellmann and Sabine Seidler, editors, Polymer Testing, pages 73–231. Carl Hanser Verlag GmbH & Co. KG, München, 10 2013.

[14] Lauren Safai, Juan Sebastian Cuellar, Gerwin Smit, and Amir A. Zadpoor. A review of the fatigue behavior of 3D printed polymers. Additive Manufacturing, 28:87–97, 8 2019.

[15] R.J. Crawford and P.P. Benham. Some fatigue characteristics of thermoplastics. Polymer, 16(12):908–914, 12 1975.

[16] Kim C. Dao and Dennis J. Dicken. Fatigue failure mechanisms in polymers. Polymer Engineering & Science, 27(4):271–276, 2 1987.

[17] R. J. Crawford and P. P. Benham. Cyclic stress fatigue and thermal softening failure of a thermoplastic. Journal of Materials Science, 9(1):18–28, 1 1974.

[18] I. Constable, J. G. Williams, and D. J. Burns. Fatigue and Cyclic Thermal Softening of Thermoplastics. Journal of Mechanical Engineering Science, 12(1):20–29, 2 1970.

[19] HP Development Company. HP Multi Jet Fusion technology A disruptive 3D printing technology for a new era of manufacturing, 2018.

[20] Kok Peng Marcian Lee, Chrysoula Pandelidi, and Mladenko Kajtaz. Build orientation effects on mechanical properties and porosity of polyamide-11 fabricated via multi jet fusion. Additive Manufacturing, 36:101533, 12 2020.

[21] Chrysoula Pandelidi, Kok Peng Marcian Lee, and Mladenko Kajtaz. Effects of polyamide-11 powder refresh ratios in multi-jet fusion: A comparison of new and used powder. Additive Manufacturing, 40, 4 2021.

[22] Wei Shian Tey, Chao Cai, and Kun Zhou. A Comprehensive Investigation on 3D Printing of Polyamide 11 and Thermoplastic Polyurethane via Multi Jet Fusion. Polymers, 13(13):2139, 6 2021.

[23] Robert McNeel and Others. Rhinoceros 3D, Version 7, 12 2023.

[24] Edith M. Arnold, Samuel R. Ward, Richard L. Lieber, and Scott L. Delp. A model of the lower limb for analysis of human movement. Annals of Biomedical Engineering, 38(2):269–279, 2 2010.

[25] Alireza Nouri, Lijing Wang, Yuncang Li, and Cuie Wen. Materials and Manufacturing for Ankle–Foot Orthoses: A Review. Advanced Engineering Materials, 25(20), 10 2023.

[26] ASTM International. ASTM Standard D790-17 Standard Test Methods for Flexural Properties of Unreinforced and Reinforced Plastics and Electrical Insulating Materials. ASTM International, 2017.

[27] ASTM International. ASTM Standard D7774-17 Standard Test Method for Flexural Fatigue Properties of Plastics. ASTM International, 2017.

[28] Elisa S. Schrank, Lester Hitch, Kevin Wallace, Richard Moore, and Steven J. Stanhope. Assessment of a Virtual Functional Prototyping Process for the Rapid Manufacture of Passive-Dynamic Ankle-Foot Orthoses. Journal of Biomechanical Engineering, 135(10), 10 2013.

[29] Dassault Systèmes Simulia Corp. (2023). Abaqus (Version 2023), 2023.

[30] M Kajtaz and K P M Lee. Finite Element Modelling of Additive-Manufactured PA11. In 13th International Conference on the Mechanical Behaviour of Materials (ICM13), pages 37–42, 2019.

[31] G M Swallowe. Strain Rate Effects. In G M Swallowe, editor, Mechanical Properties and Testing of Polymers: An A–Z Reference, pages 214–218. Springer Netherlands, Dordrecht, 1999.

[32] Panagiotis E. Chatzistergos, Nicola Eddison, Evangelia Ganniari-Papageorgiou, and Nachiappan Chockalingam. A quantitative analysis of optimum design for rigid ankle foot orthoses: The effect of thickness and reinforcement design on stiffness. Prosthetics & Orthotics International, 6 2023.